JOM, Vol. 65, No. 9, 2013
DOI: 10.1007/s11837-013-0699-8

Studies of Materials at the Nanometer Scale Using Coherent X-Ray Diffraction Imaging

RICHARD L. SANDBERG,[1,5] ZHIFENG HUANG,[2] RUI XU,[2] JOSE A. RODRIGUEZ,[3,4] and JIANWEI MIAO[2]

1.—Laboratory for Ultrafast Materials and Optical Sciences, Center for Integrated Nanotechnologies, Los Alamos National Laboratory, Los Alamos, NM 87544, USA. 2.—Department of Physics and Astronomy, and California NanoSystems Institute, University of California, Los Angeles, CA 90095, USA. 3.—Department of Biological Chemistry, UCLA-DOE Institute for Genomics and Proteomics, University of California, Los Angeles, CA 90095, USA. 4.—Howard Hughes Medical Institute (HHMI), Chevy Chase, MD 20815-6789, USA. 5.—e-mail: sandberg@lanl.gov

For many years, x-ray microscopy has been attractive for materials studies with its ability to image thick samples and provide nanometer-scale resolution. However, the ability to manufacture high-resolution x-ray optics has been a hurdle to achieving the full potential of diffraction limited x-ray imaging. Recently, the advent of bright and coherent x-ray sources at synchrotrons and x-ray free electron lasers has enabled a lensless imaging technique called coherent diffractive imaging (CDI). Since it was first demonstrated in 1999, CDI has been rapidly developing into a materials imaging technique with resolutions approaching a few nanometers. This review provides an overview of the development of CDI and several applications to nanometer-scale imaging in two and three dimensions of biological and condensed mater materials. Also, we review the development of tabletop, coherent, soft x-ray sources that provide a complimentary and potentially more accessible source for nanometer-scale coherent imaging of materials.

INTRODUCTION

Microscopy has revolutionized our understanding of nature by allowing us to visualize the world beyond the limited resolution imposed by the human eye. Optical, fluorescence, phase-contrast, confocal, x-ray, and electron microscopies are widely used in the science of materials. These lens-based microscopies are limited in their resolution by both the lenses they employ and the wavelength of their light or electron source. In visible light microscopes, lenses are solid, precision-shaped glass, while magnetic fields are used for focusing electrons and x-ray optics used for focusing x-rays. High-frequency information not collected by the lens is excluded from the formed image, while collected light is subject to lens imperfections, which introduce aberrations into the image. Collectively, these limits on visible light microscopy constrain its resolution to within the range of 200 nm, although state-of-the-art, fluorescence based super-resolution optical microscopy can achieve resolutions of 20 nm.[1,2] Transmission electron microscopy can achieve atomic resolution, but it is limited by sample thickness, which must remain thinner than 50 nm.[3] X-rays have the advantage of longer penetration depths, which can be exploited to image thicker samples. However, x-rays are more difficult to focus than electrons and visible light, and currently the highest image resolution achievable by x-ray optics is in the 10-nm range.[4,5]

One strategy for eliminating the constraints of lenses in imaging is the use of coherent diffraction imaging (CDI), also termed "coherent diffraction microscopy" or "lensless imaging." First suggested by Sayre[6,7] and demonstrated experimentally by Miao in 1999,[8] CDI collects a continuous and oversampled far-field diffraction pattern produced when a coherent x-ray beam impinges on an isolated sample. The diffraction pattern collected is inverted through a computer-enabled phasing process to obtain a high-resolution image of the sample. In principle, the final image can be aberration free and its resolution is only diffraction and dose limited.

(Published online August 10, 2013)

Figure 1 illustrates the schematic employed in the first CDI experiment and its results.[8]

In the experiment illustrated in Fig. 1a, a 10-μm pinhole placed in front of the sample generated a coherent incident x-ray beam with a wavelength of 1.7 nm, from an undulator beamline at the National Synchrotron Light Source (Brookhaven, NY). A liquid-nitrogen–cooled charge-coupled device (CCD) camera was used to collect an oversampled far-field diffraction pattern by accumulating a large number of individual exposures to enhance the dynamic range and the signal-to-noise ratio of diffraction patterns for phase retrieval.

Since this first experiment, CDI has been widely applied to a variety of science and industry applications[9–18] and used to investigate the structure of a variety of samples including nanoparticles, nanocrystals, and biomaterials, using synchrotron radiation,[19–58] high harmonic generation (HHG) sources, soft x-ray lasers,[59–65] free-electron lasers,[66–72] and coherent electron beams.[73–79] The fundamental principles of CDI have also been combined with other technologies and physical principles in techniques such as Bragg CDI;[17,41,42,57] scanning CDI;[36,49,80] Fresnel CDI;[25,32] "polyCDI," which uses a broadband source;[81] CDI in reflection geometry;[82] and others.[83,84]

BASIC PRINCIPLE OF CDI

Oversampling Theory

The phase problem is a longstanding phenomenon that refers to the loss of phase information when recording diffraction events by conventional means such as film, a CCD detector, or modern x-ray pixel array detectors. The phase problem limits measurements using visible optics, x-rays, electrons, and neutrons.[85] In CDI, diffracted x-rays are measured such that only their intensities are recorded, producing a systematic loss of phase information in measured diffraction patterns, which can be interpreted as the modulus of a Fourier transform of the specimen's electron density. The phase of this Fourier transform is lost during measurement, and without this phase information, the object function cannot be reconstructed by direct inversion of the recorded pattern.

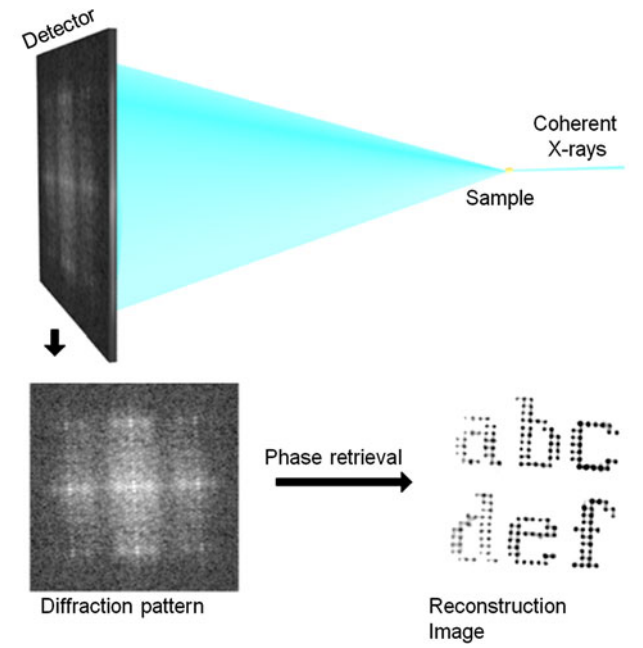

Fig. 1. First experiment of the coherent diffraction imaging (Reprinted figure with permission from Ref. 8, Copyright © 1999 by the Macmillan Publishers Limited).

In x-ray crystallography, diffraction patterns are composed of sharp, sparse Bragg peaks;[86] however, in 1952, Sayre reasoned that the lost phase information of a scattered x-ray wave might be recovered if the intensity between the Bragg peaks of a diffraction pattern were measured. This reasoning came from the fact that the autocorrelation function of an object is exactly twice the size of the object,[87] which according to the well-known Nyquist–Shannon sampling theorem is sufficient to uniquely determine the structure of an object.[88] Several studies[89–91] subsequently proved that phases could be uniquely retrieved from the intensities of a diffraction pattern if and only if the pattern was sampled at a frequency twice finer than the Nyquist interval. That means the diffraction pattern should be oversampled at a rate finer than the inverse of the sample size, by at least a factor of 2 in each dimension.

In 1998, Miao et al. reasoned that since diffraction patterns obtained from noncrystalline objects in CDI are continuous and weak, it should be possible to uniquely retrieve the structure of an object from its diffraction pattern alone without oversampling this pattern by twice in each dimension.[92] For phase retrievals of 2D and 3D objects, the oversampling ratio (σ.) was introduced to characterize the degree of oversampling:[92]

$$\sigma = \sigma_x \sigma_y \sigma_z$$

where σ_x, σ_y, and σ_z represent the sampling frequency divided by the Nyquist interval in the x, y, and z axis, respectively. When $\sigma > 2$, the number of measured correlated intensity points is more than the number of unknown variables and the phase problem can be solved uniquely in principle. This principle was later demonstrated experimentally by Miao and colleagues.[8,93]

Phase Retrieval Algorithms

A number of iterative algorithms have been developed to recover the phase information from oversampled diffraction patterns, including the hybrid input–output (HIO),[94,95] error reduction (ER),[95] difference map,[96] Hamiltonian,[97] shrink-wrap,[98] and guided HIO (GHIO)[99] methods among others. These algorithms iterate back and forth between real and reciprocal space.

Hybrid input–output, which is based on the framework of Gerchberg and Saxton,[100] is currently the most widely used phase retrieval algorithm. HIO can faithfully retrieve the phase of an ideal oversampled diffraction pattern, but in the case of experimental data, it is often trapped in local minima of the solution space. GHIO, which combines HIO with a guided approach,[101] can facilitate the location of a global minimum and therefore can retrieve lost phase information from diffraction intensities with much better accuracy.[99] Efforts to streamline and optimize phase retrieval algorithms continue to date; they include deconvolution[102] and wavelet domain constraints,[103] as well as benchmarks for guaranteeing the acquisition of high-quality diffraction patterns.[104] Ankylography has been proposed as a special method to reconstruct the 3D structure of an object from a single 2D spherical pattern.[63] Despite these advances, it remains a challenge to reconstruct fine features in weakly scattering objects, such as organic specimens, from noisy diffraction data despite large oversampling ratios.

Recently, a noise robust framework was introduced to improve the performance of HIO in the face of experimental noise,[105] and we have proposed an effective iterative algorithm, termed oversampling smoothness (OSS), for phase retrieval from noisy diffraction intensities.[106] OSS exploits the fact that in ideal cases, the region outside the support is assumed to be zero, but in practice, it reflects the character of the noise profile contaminating the diffraction intensities. OSS applies a general constraint to this region by means of a convolution with a proper filter at different stages of the iterative process, which is equivalent to the application of a tunable spatial frequency filter to the region outside the support. In doing so, i.e., by introducing a smoothness constraint, OSS finds a balance between the HIO and ER algorithms to search for a global minimum in solution space, while reducing potential pitfalls in reconstruction due to noisy diffraction data. OSS initiates 100 independent reconstructions with random initial phases. Each of these reconstructions then iterates back and forth between real and reciprocal space a total of 2000 times.

For noisy data, OSS consistently delivers reconstructions with lower errors than HIO, and ER–HIO algorithms, and outperforms most algorithms in terms of accuracy and consistency of the reconstructions.

These algorithms are fit for the recovery of phases from diffraction amplitudes obtained from isolated objects. However, these approaches are not suitable for nonisolated continuous objects. In the latter case, ptychographic CDI allows for the implementation of scanning x-ray diffraction microscopy for nonisolated or large-sized specimens by collecting diffraction patterns with a localized illumination probe from overlapping regions of a specimen.[36,49] Another approach to imaging nonisolated objects is through illuminating the object with a known, highly curved wavefront that provides an additional constraint in the phase retrieval.[32,107] Since the illumination or probe beam is known, its effects can be accounted for and thus extended objects can be measured.

MATERIALS SCIENCE STUDIES AT SYNCHROTRONS

Summary of Biological Imaging Results

Because x-ray wavelengths are on the order of the size of atoms and x-rays have a longer penetration depth than electrons, x-ray CDI has been applied to the structural determination of a variety of organic materials. By avoiding the use of lenses and overcoming the limitations imposed by x-ray optics, the first biological CDI experiment was demonstrated by imaging of *Escherichia Coli* bacteria in 2003.[21] Subsequently, CDI has been successfully used to image yeast cells,[29,34,44,58] protein crystals,[108] fish bone,[33] virions,[37] and a human chromosome,[38] at the nanometer scale.

Coherent diffractive imaging has been implemented to interrogate the structure of mineral crystals inside biological composite materials (i.e., skeletal fish bone) with spatial resolution in the nanometer scale.[33] Bone mineral crystals in collagen fibrils at different stages of mineralization were identified using CDI, which is consistent with small-angle x-ray scattering results from the same bone samples. Supported by biomineralization analyses, CDI helped reveal a dynamic model of the nucleation, growth, and orientation of mineral crystals in the collagen matrix at different stages of mineralization.

Another powerful example of CDI was the effort to reveal the structure of one of the smallest organic particles imaged by CDI; quantitative and high-contrast imaging of a single murine herpesvirus-68 virion was achieved by use of x-ray diffraction microscopy at SPring-8.[37] The size of the virion was estimated to be 200 nm, and the quantitative structure of the viral capsid inside the virion was visualized with a spatial resolution of 22 nm.

Recently, the first 3D structure determination of a whole, unstained cell was obtained using CDI at a resolution of 50–60 nm.[34] A set of 25 complete 2D diffraction patterns were collected by tilting the sample from 69.4° to −69.4°, with a total radiation dose incurred by the sample estimated to be 5.25×10^8 Gy. From this quantitative 3D reconstruction, the morphology and structure of cellular organelles including its cell wall, vacuole, endoplasmic reticulum, mitochondria, and granules were revealed. This structure also revealed a protrusion emanating from the reconstructed yeast spore, suggesting the spore had begun its germination process, as illustrated in Fig. 2a.

Applications to Materials

Coherent diffractive imaging is an ideal tool to inspect the inner structures of a variety of materials at the nanometer scale, including materials that would be difficult to explore or impossible to visu-

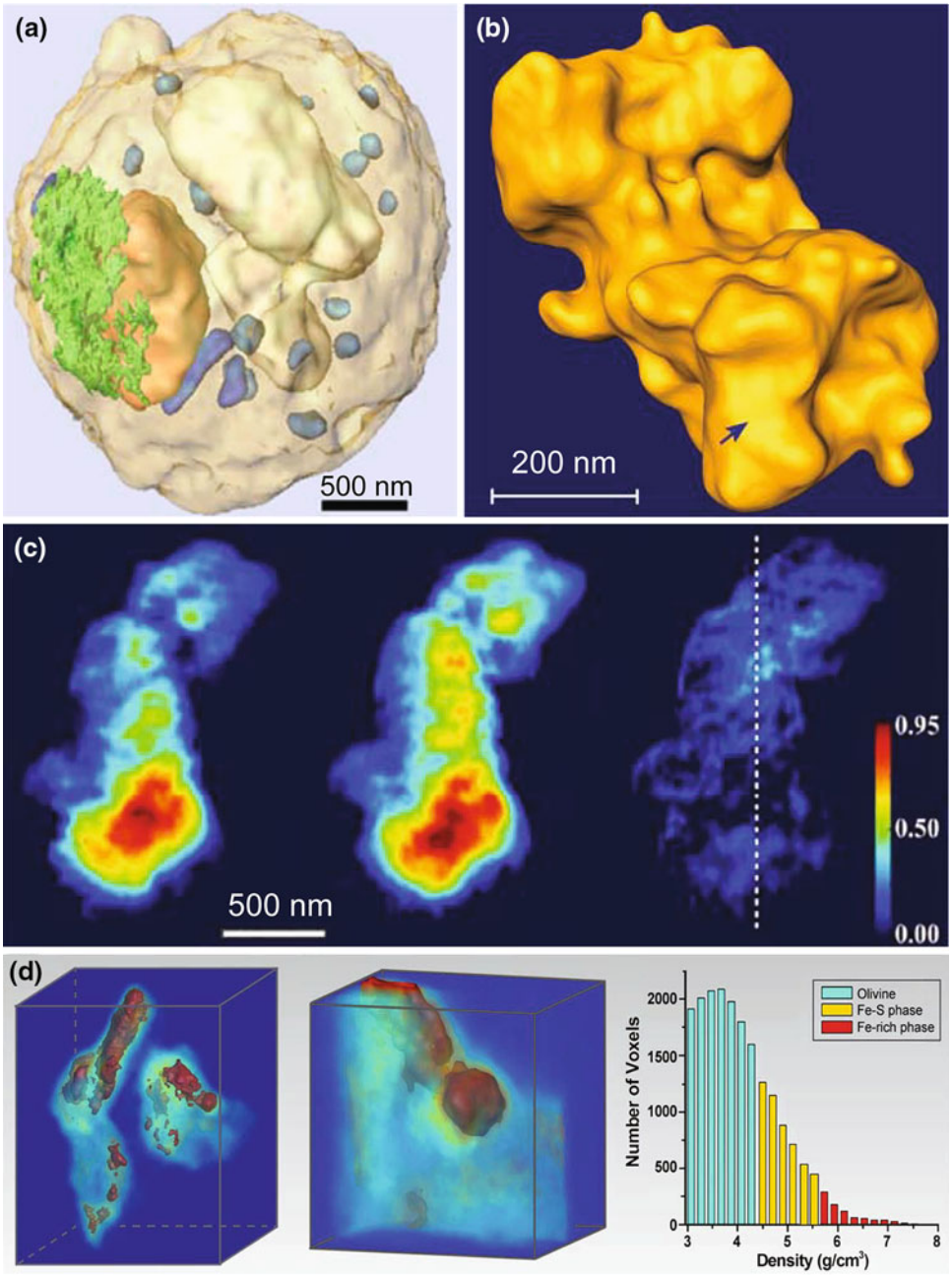

Fig. 2. Different demonstrations of CDI for nanoscale materials: (*a*) A 3D volume rendering of the reconstructed yeast spore, showing nucleus (orange), ER (green), vacuole (white), mitochondria (blue), and granules (light blue) (Scale bar: 500 nm).[34] (*b*) Isosurface rendering of a reconstructed 3D GaN quantum dot particle. The size of the platelet indicated by a blue arrow was 260 × 120 × 50 nm^3. The formation of small islands on the surface of the particles was clearly visible (some of them are labeled with green arrows).[23] (*c*) Elemental mapping of Bi structure is shown in two independently reconstructed images for each coherent x-ray diffraction pattern. From left to right: the diffraction pattern with E = 2.550 keV, the diffraction pattern with E = 2.595 keV, and the distribution of the Bi structure obtained by taking the difference of the two images.[37] (*d*) The 3D melted composition and distribution in the olivine and molten Fe–S sample. From left to right: 3D volume rendering of the olivine-Fe–S sample, showing the Fe-rich phase, Fe–S phase, and olivine distribution; a zoomed view of a 600 × 600 × 600 nm^3 volume inside the olivine-Fe–S sample; a histogram of the Fe-rich phase, Fe–S phase, and olivine distribution in the zoomed view[35] (Color figure online).

alize by other means, including electron microscopy. Electron dense materials thicker than a few hundred nanometers in size have been imaged using CDI. Several examples include GaN quantum-dot nanoparticles,[22,23] ceramic nanofoam,[50] buried Bi structures inside a Si crystal,[109] strain in a single ZnO nanorod[42] and ZnO nanostructures,[51] silver nanotubes,[48] defects in colloidal crystals,[46] magnetic structures of an amorphous terbium–cobalt thin film,[53] the bending of silicon-on-insulator nanowires,[55] nanoscale strain evolution inside a gold single crystal during compression within a diamond-anvil cell,[57] molten Fe-rich alloy, and crystalline olivine samples.[35]

The 3D structure of a GaN quantum-dot nanoparticle was obtained using CDI, illustrating the unique ability of x-ray diffraction microscopy for revealing the structures of nanomaterials.[22,23] GaN nanoparticles in a flowing stream of N2 gas were heat treated at 900°C for 24 h, in order to oxidize the GaN particles at a controllable rate and form a thin shell of Ga oxide on the GaN core. A single, isolated GaN nanoparticle was then imaged by recording 27 oversampled diffraction patterns as the GaN particle was rotated from −69.4° to +69.4°. From this data, a 3D transform was assembled and reconstructed using the GHIO algorithm combined with the equally sloped tomography (EST) method.[110] The reconstructed particle was revealed at an isotropic resolution of 17 nm,[3] as shown in Fig. 2b. A distinctive feature of the particle is the platelet-like structure. The particle consists of a few platelets at different orientations. The formation of small islands with varied size on the surface of the particle was also observed, which was a result of the surface oxidation of GaN platelets after the heat treatment.

By combining spectroscopy with x-ray diffraction microscopy, i.e., resonant absorption x-ray diffraction microscopy, quantitative and element-specific imaging of buried structures at the nanometer scale has been demonstrated.[109] The sample was a single silicon nanocrystal with buried bismuth structures and was generated by doping Bi onto a 1-μm-thick film of Si. The sample was grown at a temperature of 300°C by using molecular beam epitaxy to co-deposit Bi and Si atoms together on top of a Si:Ge buffer layer on a Si (001) wafer. This sample was heavily doped with a density of $\sim 5 \times 1020$ cm^{-3} of Bi. The Si:Ge buffer layer was chemically dissolved using a poly-silicon etchant to separate the doped Si layer from the Si wafer. Coherent x-ray diffraction patterns were then acquired from the Bi doped Si particle sample at x-ray energies of 2.550 keV and 2.595 keV, just below and above the Bi M5 edge, respectively, with a pixel resolution of ∼15 nm as shown in Fig. 2c. Difference patterns acquired at these two energies represented the spatial distribution of the buried Bi dopant structure. We observed that the Bi atoms are broadly dispersed, which is consistent with their weak segregation tendencies.

Another example of a 3D structure revealed by CDI is that of a molten iron-rich alloy of a crystalline sample of olivine.[35] An isolated nanoparticle synthesized at 6 GPa and 1800°C was imaged by collecting 27 x-ray diffraction patterns of the sample with a tilt range of −69.4° to 69.4°, with each 2D diffraction pattern with a per-pixel resolution of 16.3 nm. A set of 2D images retrieved by the OSS algorithm was used to reconstruct a 3D image by the EST method, with an isotropic spatial resolution of ∼32.5 nm in x–y and ∼48.8 nm in z. Figure 2d illustrates the 3D distribution of the Fe-rich and Fe–S phases in the olivine–Fe–S sample and indicates that the Fe-rich melt exhibits varied 3D shapes and sizes within the olivine matrix. This experiment not only further demonstrates the capability of applying CDI to structural studies of materials but also expands our comprehensive understanding of the structural and morphological features of materials under high pressures and temperatures.

NANOMETER-SCALE COHERENT DIFFRACTION IMAGING FROM TABLETOP SOURCES

While CDI has shown great promise in materials science at third- and fourth-generation light sources, there have been some limitations in its broader adoption due to limited access. Third-generation synchrotron sources, while providing great flexibility as x-ray probes, lack the fundamental spatial coherence needed for CDI and thus their beams must be spatially filtered. Fourth-generation light sources (so called x-ray free electron lasers or XFELs) are preferred for CDI experiments, but access and time allotted at the limited number of spatially coherent synchrotron beamlines and XFELs has hindered the development and broader application of CDI.

Over the last two decades, tabletop sources have been developed that delivers tabletop soft x-rays (photon energy range of 20–1.5 keV)[11,111] and promises to further advance CDI by making the technique more convenient and accessible. Due to the numerous core atomic resonances in the soft x-ray radiation range, elemental specific absorption contrast imaging has been used extensively; however, this also leads to limited penetration depth requiring that these sources be used in vacuum.[111] The two tabletop sources that have been the most useful at producing bright, coherent, soft x-rays have been the nonlinear upconversion of femtosecond laser light through a process called HHG[112,113] and soft x-ray lasers from highly ionized, highly dense plasmas that are produced either through electrical discharge or by pumping a solid target with intense lasers.[111,114,115] In this section, we will review these tabletop sources, nanometer-scale tabletop demonstrations of CDI with wavelength limited resolution (∼20 nm) in 2D and 3D, as well as the outlook for how developments in these sources will soon enable ultrafast time-resolved imaging of nanoscale materials.

The development of tabletop soft x-ray sources has progressed hand in hand with ultrafast laser technology over the last two and a half decades. Ultrafast lasers have enabled the highly nonlinear optical processes that produce a bright, narrowly diverging, coherent SXR beam.[116–118] Arguably, the most widely used ultrafast laser system used in producing tabletop SXR sources are titanium-doped sapphire lasers (Ti:Sapph), which typically operate at a wavelength of 800 nm and are capable of pro-

ducing single optical cycle (few femtosecond) pulses.[116,118] These intense (Petawatt to Terrawatt scale) lasers range from the few mJ up to 1 J in pulse power and are capable of producing highly ionized plasmas that are the source of both the SXR laser and HHG. While SXR are often produced by rapidly ionizing solid targets with optical lasers, they can also be produced with fast electrical discharges through gas-filled capillaries (typically argon and neon).[111,114] In these very dense plasmas, the highly ionized atoms are "pumped" electrically by the plasma collisions into highly excited states (neon-like argon or nickel-like silver) and an electronic population inversion occurs allowing for single-pass SXR lasing. These sources can produce extremely intense (>1-mJ pulse energy), highly monochromatic (bandwidths $\lambda/\Delta\lambda \sim 10^5$), nanosecond pulses in the 10–50-nm wavelength range. SXR lasers have been applied extensively to coherent nanoscale imaging.[115,119–121] However, they suffer from limited spatial coherence due to their single-pass nature and lack of an optical cavity. Recently, these limitations have been overcome through the use of spatial filtering or seeding from an HHG source; in such configurations, they can produce fully coherent, intense beams.[120,122]

While SXR lasers can produce more intense x-ray beams and were thus the first to be applied to tabletop coherent imaging,[123] the nonlinear upconversion of femtosecond lasers into the SXR through HHG provides a compelling complimentary approach for CDI experiments. HHG offers the ability to produce femtosecond to attosecond (10^{-18} s) pulses that are inherently spatially coherent, and it has the ability to scale more easily to higher photon energies (>1 keV), all of which are important for practical materials science applications.[112,113,124–127] HHG typically involves focusing intense, femtosecond pulses of near-infrared (IR) light into a low-pressure (1–100 Torr) noble gas (He, Ne, Ar) in either a gas-jet, gas-cell, or gas-filled waveguide geometry.[117,118,128,129] The generation of the SXR beam has been compared with the coherent version of the Roentgen x-ray tube that uses electric fields to accelerate electrons from a cathode into an anode, thus, producing high-energy photons in the x-ray range. However, in HHG, the intense driving laser field ionizes the gas atoms in the target and then accelerates the electrons back into the parent ion on every half cycle of the driving laser, thus, producing high-energy SXR photons in attosecond bursts.[130,131] This HHG process produces a comb of odd laser harmonics spaced by ~3-eV photon energies and can extend up to several thousand harmonics into the 1-keV photon range.[124,132] Because a coherent laser drives the HHG process, the SXR radiation maintains this spatial coherence, especially when the nonlinear upconversion process is phase matched.[113,132–137]

SXR laser-based imaging experiments were the first successful attempts at using tabletop sources for coherent imaging, but their reconstructions suffered from low resolution (limited to several μs) due to the holographic techniques used and the limited spatial coherence of the source.[123] A few years later, Bartels et al.[113] demonstrated comparable resolution imaging by in-line holography on a 32-nm HHG source.

Over the next several years, both SXR lasers and HHG sources were used in holographic techniques and with Fresnel zone plate lenses to produce images with resolution down to half a μm. However, these experiments produced images that were still far from wavelength limited.[138–141] The first demonstration of coherent diffractive imaging, which produced images with resolutions only limited by the wavelength and scattering angle, was achieved in 2007 by Sandberg et al.[59,142] In these experiments, a phase-matched, 32-nm HHG source was applied at normal incidence to a test object in order to obtain ~200–nm resolution of a gold-coated carbon TEM grid that was placed onto a 15-μm pinhole as shown in Fig. 3. Also shown in Fig. 3 is a typical experiment geometry for many tabletop SXR coherent microscopes. The coherent, tabletop SXR beam is spectrally filtered from the driving laser light or plasma emission by transmitting the beam through thin (100–200-nm) metal filters. Often, normal incidence dielectric-coated mirrors are used to focus the beam (and sometimes monochromotize it as in the case of HHG) on the sample. Finally, a large-area, SXR-sensitive CCD is used to collect the diffracted light. Occasionally, beam blocks are used to block out the most intense part of the scattered light in order to overcome the limited dynamic range of the detectors.

Since its first demonstrations, CDI using tabletop sources has advanced rapidly into nanoscale imaging (sub-100-nm resolution). Using a similar system as shown in Fig. 3, Sandberg et al.[60] demonstrated near-wavelength-limited CDI with a spatially filtered 46.9-nm capillary discharge SXR laser and with the 32-nm HHG source (see Fig. 4a). The sample was a 7-μ-tall stick figure cut out of a silicon nitride membrane by electron beam lithography. By moving the detector much closer to the sample and increasing the flux of the source, the 32-nm HHG source produced a 90-nm resolution image in an 80-minute exposure by integrating the 1-kHz repetition rate source over many shots. In a similar high numerical aperture (NA = 0.6) scheme to capture large scattering angles, the SXR laser produced 70-nm resolution with an integration of about 5 min at a 1-Hz repetition rate. In recent years, this resolution was pushed down to 50 nm with the same 32-nm HHG source (but with improved flux of about[108] photons per second on the sample)[61] and down to 20-nm resolution with a 13-nm HHG source in only 20 min of exposure.[64] At these shorter wavelengths (at and below 10 nm), penetration depths in materials become longer and numerous materials applications begin to open including mask inspection for

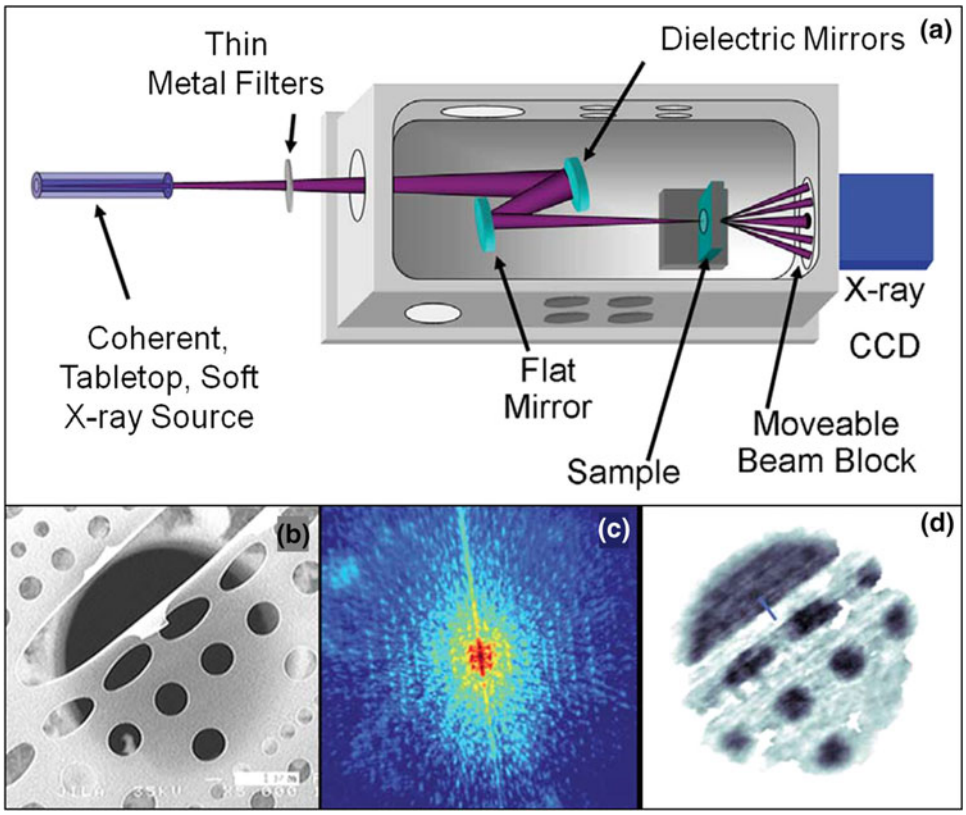

Fig. 3. (Top) Schematic of typical tabletop coherent imaging setup: A coherent tabletop SXR source (in vacuum) is filtered by thin metal filters and focused onto a sample stage. A large-area SXR CCD camera collects the diffraction pattern. (Bottom) Demonstration of first tabletop CDI from a 29-nm high harmonic generation source: (a) SEM image of gold-plated carbon TEM grid placed on a 15-μm-diameter pinhole, (b) recorded multiframe 29-nm diffraction pattern, and (c) CDI reconstruction of transmission image of TEM grid and pinhole with 214-nm resolution (Reprinted figure with permission from Ref. 59, Copyright © 2007 by the American Physical Society).

next-generation extreme ultraviolet computer chip lithography, biological imaging of whole cells, and materials damage studies.[111] In this high NA scheme, resolution is limited only by the available flux and wavelength of the incident x-rays. However, the curvature effects of high-angle-scattered photons incident on the flat detector must be taken into account and corrected in order to avoid distortion of the diffraction pattern. This effect can be corrected by mapping the diffraction pattern sampled on the flat CCD onto a curved surface that is an equal distance from the sample. This correction can be seen in Fig. 4a where the corners of the diffraction pattern (high scattering angle) are pulled in due to the increased angle incident on the detector.[60] This effect has exciting implications to imaging, which will be discussed later.

While still limited by integration time and available wavelength, these initial applications of tabletop CDI have already led to some interesting applications such as imaging nanomaterials,[120,138,140] and nanopatterned surfaces in reflection mode.[143] In particular, the ultrafast SXR pulses and available photon energy (10–100 eV) of HHG make it an ideal source for studying ultrafast magnetization dynamics in many magnetic materials as their M-absorption edges fall in this region.[111] Figure 4b shows a typical phase-matched HHG spectrum from neon (top) and the normalized transmission edges of several common magnetic materials with M-edges in this energy range.[144] These powerful attributes of HHG have already lead to several significant spectroscopic studies of magnetic thin films that have lead to novel insight about the ultrafast coupling among spin, charge, and lattice degrees of freedom in these materials.[145–149] Currently, many groups around the world are pursuing nanometer-scale imaging of magnetic domains with tabletop SXR sources.

While tabletop CDI has had some very intriguing preliminary applications to materials science imaging, to become a practical tool, exposure times will have to be shortened significantly below the >10 min per exposure that has been demonstrated currently by HHG with kHz repetition rate lasers. This is especially true for studies of dynamic events, which are abundant in current materials science. While other tabletop sources have demonstrated sub-100-nm resolution in a single shot previously,[119,150] the first nanoscale (100 nm) coherent imaging in a single exposure pulse was demonstrated by Ravasio et al.[62] in 2009 where they used a large-scale HHG source with upward of 10^9 coher-

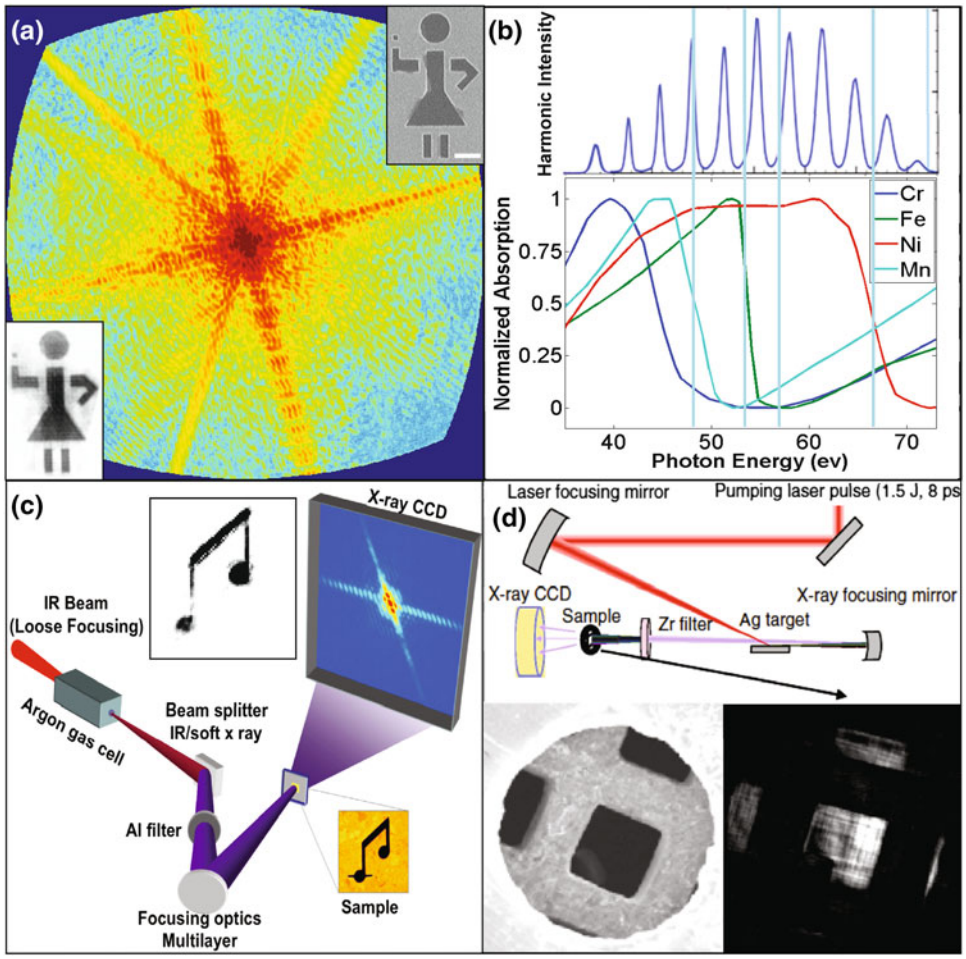

Fig. 4. Various demonstrations and applications of tabletop SXR coherent imaging: (a) Curvature corrected, high-numerical-aperture diffraction pattern of 47-nm SXR laser illuminated stick figure with 70-nm resolution (top inset - SEM image of 7-μm high figure, bottom inset – CDI reconstruction);[60] (b) HHG spectrum from neon (top) and normalized transmission curves of several magnetic materials at their M-absorption edge (bottom) demonstrating the applicability of HHG sources to studying magnetic materials;[144] (c) 100-nm-resolution, single-shot CDI image of "notes" pattern from an single pulse from an intense 32-nm high harmonic generation source;[62] (d) Single-shot, 13.9-nm SXR laser images of apertured gold mesh on a 20-μm pinhole with 194-nm resolution[152] (Reprinted figures with permission from (c) Ref. 62, Copyright © 2009 by the American Physical Society; and (d) Ref. 152, Copyright © 2012 by the Optical Society of America).

ent SXR photons (32 nm) on the sample in a single 20-fs pulse. The experimental setup and recovered single-shot image are shown in Fig. 4c. This demonstration opens the way for routine single-shot, nanometer-scale SXR imaging that will be only limited by the wavelength and available flux, making experiments feasible that are currently only achievable by using large XFEL facilities. Since this first demonstration, other groups have also performed nanoscale, single-shot coherent imaging on various tabletop sources such as laser-driven SXR sources (Fig. 4b).[151–153]

In addition to single-shot imaging, another interesting and powerful imaging technique that has come from the development of tabletop SXR coherent imaging is single-view, three-dimensional imaging or "anklyography."[63] The idea of this 3D imaging was first discussed in the literature in 2007 and 2009 as a result of the extremely high numerical apertures imaging that was being demonstrated.[154,155] However, it was not until the "curvature correction" of the distorted 0.6 NA SXR diffraction pattern was first fully understood (Fig. 4a) that the ability to image in 3D was demonstrated. The basic principle behind this technique, termed "ankylography," is that diffraction patterns at high scattering angles in Fourier space actually lie on a hemispherically curved surface known as the Ewald sphere. Due to this curvature in Fourier space, there is actually a sampling of the object in all three dimensions. For low scattering angle data, the curvature on the Ewald sphere can largely be ignored, but at larger angles, the effects of 3D information become increasingly important. When this 3D information was accounted for in the phase retrieval reconstruction from the 7-μ stick figure (Fig. 5a and Ref. 60), a three-dimensional image of the sample was obtained with 80-nm

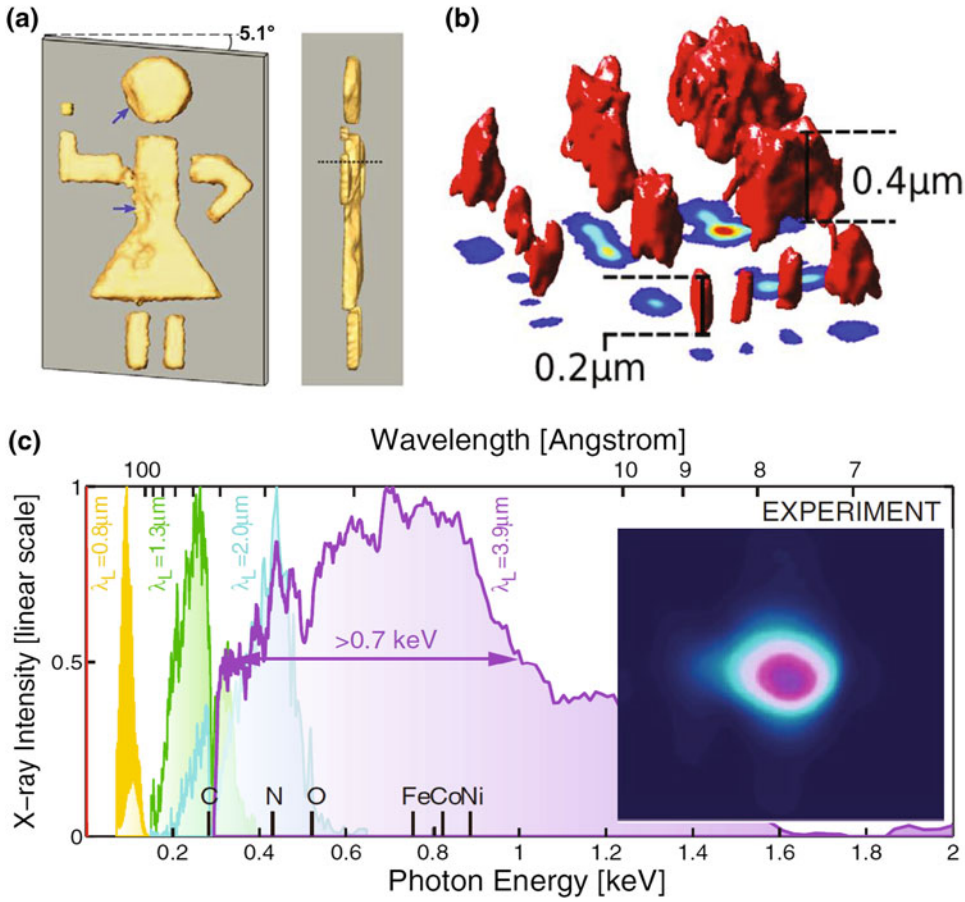

Fig. 5. The future of tabletop CDI: High-numerical-aperture CDI from tabletop sources has enabled single-view/single-shot 3D imaging ("ankylography"). (a) 3D single-view reconstruction of stick figure from a high NA diffraction pattern recorded with a 47-nm SXR laser (Fig. 4a);[63] (b) 3D single view reconstruction of resolution pattern from a 13-nm HHG source;[64] (c) Novel long wavelength driven HHG source can produce much higher energy photons (up to 1.5 keV) that will be more useful for materials imaging while still producing high-quality, intense, coherent beams (inset)[127] (Reprinted figures with permission from (a) Ref. 63, Copyright © 2010 by the Macmillan Publishers Limited; (b) Ref. 64, Copyright © 2011 by the Optical Society of America; and (c) Ref. 127, Copyright © 2012 by the American Association for the Advancement of Science).

lateral resolution (x–y) and 140-nm resolution along the propagation direction of the beam (z) as shown in Fig. 5a.[63] While the applicability of this result to larger samples or harder x-ray sources may be limited, several other demonstrations have been published including a 3D image of a test pattern from a 13-nm HHG source (Fig. 5b) and examples from a biological sample.[64,156] If the full promise of ankylography can be realized, single-shot, high-resolution imaging in 3D should be possible for lower energy sources such as tabletop SXR sources.

A limiting factor in current tabletop CDI, compared with larger, harder x-ray sources is of course the limited penetration depth of the SXR light in the state-of-the-art sources. However, in the last few years, a breakthrough in HHG has allowed much higher energy SXR photons from this femtosecond tabletop source.[112] The highest available photon energies from HHG, or so-called "cutoff" energy, scales linearly with the peak laser intensity but quadratically with the driving laser wavelength.[130,131] Therefore, one route to harder and more penetrating SXR beams is to move the driving laser wavelength from the near-IR (such as Ti:Sapph 800-nm emission) farther into the IR using various nonlinear optics techniques. This was first demonstrated in 2008 by several groups,[132,157,158] but it was Popmintchev et al. who showed that phase matching at very high gas target pressures (several atmospheres) enables bright beams with energies >1 keV.[112,159,160] Very recently, using driving femtosecond lasers with a 3.9-μm wavelength, Popmintchev et al.[127] have shown bright, phase-matched x-ray radiation up to 1.5-keV photon energies (Fig. 5c). Especially exciting for potential CDI applications in materials science, these keV sources have been shown to still maintain the full spatial coherence and excellent beam quality (Fig. 5c) necessary for coherent imaging applications.[127,160] With the demonstrated ultrafast, single-shot imaging capability and scalability to more useful SXR energies >1 keV on HHG sources, cur-

rently the stage is set for tabletop SXR CDI to have a major impact on nanoscale and ultrafast materials science applications in various fields.

OUTLOOK FOR CXDI FOR MATERIALS STUDIES

The past decade and a half has seen an explosion in coherent diffractive imaging development and applications. Since its first experimental demonstration at a synchrotron in 1999,[8] CDI continues to develop at a very rapid pace. Due to its lensless nature, CDI has been able to overcome the limitations of x-ray optics by achieving resolutions down to a few nm,[43,161] and it has demonstrated imaging of ultrafast dynamics by using single-shot CDI at fourth-generation sources.[67] Furthermore, advances in CDI as applied to electron microscopy could hold the key to overcoming resolution limits and in opening the doors to many transformative applications.[73–78,162–164] CDI has come far beyond the limitation of imaging only isolated objects with new scanning CDI techniques such as Fresnel CDI, ptychographic CDI, and apertured illumination CDI.[31,32,36] These techniques have been applied extensively to materials science problems including integrated circuits and low-density canalicular structures in bone, to name a few.[36,107] Finally, CDI has found extensive application to 3D tomographic imaging as discussed in this article.

As shown here, CDI has the unique ability to inspect nanoscale materials and is in principle only wavelength limited. As much more powerful x-ray storage rings, XFELs, and tabletop x-ray sources are being developed, the promise of achieving atomic resolution using CDI may soon be achieved with high-intensity and highly coherent x-rays. The future of CDI is bright for nanoscale materials. Resolving atomic structures of nanomaterials using CDI has been predicted by the computer simulations,[165] which could be used to one day determine 3D disordered structurels such as dislocations at atomic resolution, as has been demonstrated using electron tomography.[166,167]

REFERENCES

1. K.I. Willig, R.R. Kellner, R. Medda, B. Hein, S. Jakobs, and S.W. Hell, *Nature* 440, 935 (2006).
2. E. Betzig, G.H. Patterson, R. Sougrat, O.W. Lindwasser, S. Olenych, J.S. Bonifacino, M.W. Davidson, J. Lippincott-Schwartz, and H.F. Hess, *Science* 313, 1642 (2006).
3. J. Spence, *High Resolution Electron Microscopy* (New York: Oxford Univ. Press, 2003).
4. A. Sakdinawat and D. Attwood, *Nat. Photonics* 4, 840 (2010).
5. H. Mimura, S. Handa, T. Kimura, H. Yumoto, D. Yamakawa, H. Yokoyama, S. Matsuyama, K. Inagaki, K. Yamamura, Y. Sano, K. Tamasaku, Y. Nishino, M. Yabashi, T. Ishikawa, and K. Yamauchi, *Nat. Phys.* 6, 122 (2010).
6. D. Sayre, *Imaging Processes and Coherence in Physics*, eds. M. Schlenker, M. Fink, J.P. Goedgebuer, C. Malgrange, J.C. Vienot, and R.H. Wade, vol. 112 (Springer Lecture Notes in Physics Berlin: Springer, 1980), pp. 229–235.
7. D. Sayre, *Direct Methods of Solving Crystal Structures*, ed. H. Schenck (New York: Plenum, 1991), pp. 353–356.
8. J. Miao, P. Charalambous, J. Kirz, and D. Sayre, *Nature* 400, 342 (1999).
9. J. Miao, H.N. Chapman, J. Kirz, D. Sayre, and K.O. Hodgson, *Annu. Rev. Biophys. Biomol. Struct.* 33, 157 (2004).
10. J. Miao, T. Ishikawa, T. Earnest, and Q. Shen, *Annu. Rev. Phys. Chem.* 59, 387 (2008).
11. J. Miao, R.L. Sandberg, and C. Song, *IEEE J. Sel. Top. Quant. Electron.* 18, 399 (2012).
12. I.K. Robinson and J. Miao, *MRS Bull.* 29, 177 (2004).
13. K. Nugent, *Adv. Phys.* 59, 1 (2010).
14. H.M. Quiney, *J. Mod. Opt.* 57, 1109 (2010).
15. H.N. Chapman and K.A. Nugent, *Nat. Photonics* 4, 833 (2010).
16. A.P. Mancuso, O.M. Yefanov, and I.A. Vartanyants, *J. Biotechnol.* 149, 229 (2010).
17. M. Holt, R. Harder, R. Winarski, and V. Rose, *Annu. Rev. Mater. Res.* 43, 183 (2013).
18. A. Barty, J. Küpper, and H.N. Chapman, *Annu. Rev. Phys. Chem.* 64, 415 (2013).
19. I.K. Robinson, I.A. Vartanyants, G.J. Williams, M.A. Pfeifer, and J.A. Pitney, *Phys. Rev. Lett.* 87, 195505 (2001).
20. J. Miao, T. Ishikawa, B. Johnson, E.H. Anderson, B. Lai, and K.O. Hodgson, *Phys. Rev. Lett.* 89, 088303 (2002).
21. J. Miao, K.O. Hodgson, T. Ishikawa, C.A. Larabell, M.A. LeGros, and Y. Nishino, *Proc. Natl. Acad. Sci. USA* 100, 110 (2003).
22. J. Miao, Y. Nishino, Y. Kohmura, B. Johnson, C. Song, S.H. Risbud, and T. Ishikawa, *Phys. Rev. Lett.* 95, 085503 (2005).
23. J. Miao, C.C. Chen, C. Song, Y. Nishino, Y. Kohmura, T. Ishikawa, D. Ramunno-Johnson, T.K. Lee, and S.H. Risbud, *Phys. Rev. Lett.* 97, 215503 (2006).
24. G.J. Williams, M.A. Pfeifer, I.A. Vartanyants, and I.K. Robinson, *Phys. Rev. Lett.* 90, 175501 (2003).
25. G.J. Williams, H.M. Quiney, B.B. Dhal, C.Q. Tran, K.A. Nugent, A.G. Peele, D. Paterson, and M.D. de Jonge, *Phys. Rev. Lett.* 97, 025506 (2006).
26. G.J. Williams, E. Hanssen, A.G. Peele, M.A. Pfeifer, J. Clark, B. Abbey, G. Cadenazzi, M.D. de Jonge, S. Vogt, L. Tilley, and K.A. Nugent, *Cytom Part A* 73, 949 (2008).
27. S. Marchesini, H. He, H.N. Chapman, S.P. Hau-Riege, A. Noy, M.R. Howells, U. Weierstall, and J.C.H. Spence, *Phys. Rev. B* 68, 140101 (2003).
28. K.A. Nugent, A.G. Peele, H.N. Chapman, and A.P. Mancuso, *Phys. Rev. Lett.* 91, 203902 (2003).
29. D. Shapiro, P. Thibault, T. Beetz, V. Elser, M. Howells, C. Jacobsen, J. Kirz, E. Lima, H. Miao, A.M. Neiman, and D. Sayre, *Proc. Natl. Acad. Sci. USA* 102, 15343 (2005).
30. M.A. Pfeifer, G.J. Williams, I.A. Vartanyants, R. Harder, and I.K. Robinson, *Nature* 442, 63 (2006).
31. J.M. Rodenburg, A.C. Hurst, A.G. Cullis, B.R. Dobson, F. Pfeiffer, O. Bunk, C. David, K. Jefimovs, and I. Johnson, *Phys. Rev. Lett.* 98, 034801 (2007).
32. B. Abbey, K.A. Nugent, G.J. Williams, J.N. Clark, A.G. Peele, M.A. Pfeifer, M. de Jonge, and I. McNulty, *Nat. Phys.* 4, 394 (2008).
33. H. Jiang, D. Ramunno-Johnson, C. Song, B. Amirbekian, Y. Kohmura, Y. Nishino, Y. Takahashi, T. Ishikawa, and J. Miao, *Phys. Rev. Lett.* 100, 038103 (2008).
34. H. Jiang, C. Song, C–.C. Chen, R. Xu, K.S. Raines, B.P. Fahimian, C.-H. Lu, T.K. Lee, A. Nakashima, J. Urano, T. Ishikawa, F. Tamanoi, and J. Miao, *Proc. Natl. Acad. Sci. USA* 107, 11234 (2010).
35. H. Jiang, R. Xu, C.C. Chen, W. Yang, J. Fan, X. Tao, C. Song, Y. Kohmura, T. Xiao, Y. Wang, Y. Fei, T. Ishikawa, W.L. Mao, and J. Miao, *Phys. Rev. Lett.* 110, 205501 (2013).
36. P. Thibault, M. Dierolf, A. Menzel, O. Bunk, C. David, and F. Pfeiffer, *Science* 321, 379 (2008).
37. C. Song, H. Jiang, A. Mancuso, B. Amirbekian, L. Peng, R. Sun, S.S. Shah, Z.H. Zhou, T. Ishikawa, and J. Miao, *Phys. Rev. Lett.* 101, 158101 (2008).
38. Y. Nishino, Y. Takahashi, N. Imamoto, T. Ishikawa, and K. Maeshima, *Phys. Rev. Lett.* 102, 018101 (2009).
39. X. Huang, J. Nelson, J. Kirz, E. Lima, S. Marchesini, H. Miao, A.M. Neiman, D. Shapiro, J. Steinbrener, A. Stewart, J.J. Turner, and C. Jacobsen, *Phys. Rev. Lett.* 103, 198101 (2009).

40. E. Lima, L. Wiegart, P. Pernot, M. Howells, J. Timmins, F. Zontone, and A. Madsen, *Phys. Rev. Lett.* 103, 198102 (2009).
41. I. Robinson and R. Harder, *Nat. Mater.* 8, 291 (2009).
42. M.C. Newton, S.J. Leake, R. Harder, and I.K. Robinson, *Nat. Mater.* 9, 120 (2010).
43. Y. Takahashi, N. Zettsu, Y. Nishino, R. Tsutsumi, E. Matsubara, T. Ishikawa, and K. Yamauchi, *Nano Lett.* 10, 1922 (2010).
44. J. Nelson, X. Huang, J. Steinbrener, D. Shapiro, J. Kirz, S. Marchesini, A.M. Neiman, J.J. Turner, and C. Jacobsen, *Proc. Natl. Acad. Sci. USA* 107, 7235 (2010).
45. K. Giewekemeyer, P. Thibault, S. Kalbfleisch, A. Beerlink, C.M. Kewish, M. Dierolf, F. Pfeiffer, and T. Salditt, *Proc. Natl. Acad. Sci. USA* 107, 529 (2010).
46. J. Gulden, O.M. Yefanov, A.P. Mancuso, V.V. Abramova, J. Hilhorst, D. Byelov, I. Snigireva, A. Snigirev, A.V. Petukhov, and I.A. Vartanyants, *Phys. Rev. B* 81, 224105 (2010).
47. J. Gulden, O.M. Yefanov, A.P. Mancuso, R. Dronyak, A. Singer, V. Bernátová, A. Burkhardt, O. Polozhentsev, A. Soldatov, M. Sprung, and I.A. Vartanyants, *Opt. Express* 20, 4039 (2012).
48. R. Harder, M. Liang, Y. Sun, Y. Xia, and I.K. Robinson, *New J. Phys.* 12, 035019 (2010).
49. M. Dierolf, A. Menzel, P. Thibault, P. Schneider, C.M. Kewish, R. Wepf, O. Bunk, and F. Pfeiffer, *Nature* 467, 436 (2010).
50. A. Barty, S. Marchesini, H.N. Chapman, C. Cui, M.R. Howells, D.A. Shapiro, A.M. Minor, J.C.H. Spence, U. Weierstall, J. Ilavsky, A. Noy, S.P. Hau-Riege, A.B. Artyukhin, T. Baumann, T. Willey, J. Stolken, T. van Buuren, and J.H. Kinney, *Phys. Rev. Lett.* 101, 055501 (2008).
51. G. Xiong, X. Huang, S. Leake, M.C. Newton, R. Harder, and I.K. Robinson, *New J. Phys.* 13, 033006 (2011).
52. A. Schropp, P. Boye, A. Goldschmidt, S. Hönig, R. Hoppe, J. Patommel, C. Rakete, D. Samberg, S. Stephan, S. Schöder, M. Burghammer, and C.G. Schroer, *J. Microsc.* 241, 9 (2011).
53. J.J. Turner, X. Huang, O. Krupin, K.A. Seu, D. Parks, S. Kevan, E. Lima, K. Kisslinger, I. McNulty, R. Gambino, S. Mangin, S. Roy, and P. Fischer, *Phys. Rev. Lett.* 107, 033904 (2011).
54. A. Tripathi, J. Mohanty, S.H. Dietze, O.G. Shpyrko, E. Shipton, E.E. Fullerton, S.S. Kim, and I. McNulty, *Proc. Natl. Acad. Sci. USA* 108, 13393 (2011).
55. X. Shi, G. Xiong, X. Huang, R. Harder, and I. Robinson, *New J. Phys.* 14, 063029 (2012).
56. A.A. Minkevich, E. Fohtung, T. Slobodskyy, M. Riotte, D. Grigoriev, T. Metzger, A.C. Irvine, V. Novák, V. Holý, and T. Baumbach, *EPL* 94, 66001 (2011).
57. W. Yang, X. Huang, R. Harder, J.N. Clark, I.K. Robinson, and H. Mao, *Nat. Commun.* 4, 1680 (2013).
58. D. Nam, J. Park, M. Gallagher-Jones, S. Kim, S. Kim, Y. Kohmura, H. Naitow, N. Kunishima, T. Yoshida, T. Ishikawa, and C. Song, *Phys. Rev. Lett.* 110, 098103 (2013).
59. R.L. Sandberg, A. Paul, D.A. Raymondson, S. Hadrich, D.M. Gaudiosi, J. Holtsnider, R.I. Tobey, O. Cohen, M.M. Murnane, H.C. Kapteyn, C. Song, J. Miao, Y. Liu, and F. Salmassi, *Phys. Rev. Lett.* 99, 098103 (2007).
60. R.L. Sandberg, C. Song, P.W. Wachulak, D.A. Raymondson, A. Paul, B. Amirbekian, E. Lee, A.E. Sakdinawat, O.V.C. La, M.C. Marconi, C.S. Menoni, M.M. Murnane, J.J. Rocca, H.C. Kapteyn, and J. Miao, *Proc. Natl. Acad. Sci. USA* 105, 24 (2008).
61. R.L. Sandberg, D.A. Raymondson, C. La-o-vorakiat, A. Paul, K.S. Raines, J. Miao, M.M. Murnane, H.C. Kapteyn, and W.F. Schlotter, *Opt. Lett.* 34, 1618 (2009).
62. A. Ravasio, D. Gauthier, F.R.N.C. Maia, M. Billon, J.-P. Caumes, D. Garzella, M. Geleoc, O. Gobert, J.-F. Hergott, A.-M. Pena, H. Perez, B. Carre, E. Bourhis, J. Gierak, A. Madouri, D. Mailly, B. Schiedt, M. Fajardo, J. Gautier, P. Zeitoun, P.H. Bucksbaum, J. Hajdu, and H. Merdji, *Phys. Rev. Lett.* 103, 028104 (2009).
63. K.S. Raines, S. Salha, R.L. Sandberg, H. Jiang, J.A. Rodriguez, B.P. Fahimian, H.C. Kapteyn, J. Du, and J. Miao, *Nature* 463, 214 (2010).
64. M.D. Seaberg, D.E. Adams, E.L. Townsend, D.A. Raymondson, W.F. Schlotter, Y. Liu, C.S. Menoni, L. Rong, C.-C. Chen, J. Miao, H.C. Kapteyn, and M.M. Murnane, *Opt. Express* 9, 22470 (2011).
65. J.J. Turner, J. Nelson, X. Huang, J. Steinbrener, and C. Jacobsen, *Phys. Lett. A* 377, 1150 (2013).
66. H.N. Chapman, A. Barty, M.J. Bogan, S. Boutet, M. Frank, S.P. Hau-Riege, S. Marchesini, B.W. Woods, S. Bajt, W.H. Benner, R.A. London, E. Plonjes, M. Kuhlmann, R. Treusch, S. Dusterer, T. Tschentscher, J.R. Schneider, E. Spiller, T. Moller, C. Bostedt, M. Hoener, D.A. Shapiro, K.O. Hodgson, D. van der Spoel, F. Burmeister, M. Bergh, C. Caleman, G. Huldt, M.M. Seibert, F.R.N.C. Maia, R.W. Lee, A. Szoke, N. Timneanu, and J. Hajdu, *Nat. Phys.* 2, 839 (2006).
67. A. Barty, M.J. Bogan, S. Hau-Riege, S. Marchesini, K. Sokolowski-Tinten, N. Stojanovic, H. Ehrke, A. Cavalleri, D. Stefan, and M. Frank, *Nat. Photonics* 2, 415 (2008).
68. A.P. Mancuso, A. Schropp, B. Reime, L.M. Stadler, A. Singer, J. Gulden, S. Streit-Nierobisch, C. Gutt, G. Grübel, J. Feldhaus, F. Staier, R. Barth, A. Rosenhahn, M. Grunze, T. Nisius, T. Wilhein, D. Stickler, H. Stillrich, R. Frömter, H.P. Oepen, M. Martins, B. Pfau, C.M. Günther, R. Könnecke, S. Eisebitt, B. Faatz, and N. Guerassimova, *Phys. Rev. Lett.* 102, 035502 (2009).
69. A.P. Mancuso, T. Gorniak, F. Staier, O.M. Yefanov, R. Barth, C. Christophis, B. Reime, J. Gulden, A. Singer, M.E. Pettit, T. Nisius, T. Wilhein, C. Gutt, G. Grübel, N. Guerassimova, R. Treusch, J. Feldhaus, S. Eisebitt, E. Weckert, M. Grunze, A. Rosenhahn, and I.A. Vartanyants, *New J. Phys.* 12, 035003 (2010).
70. I. Schlichting and J. Miao, *Curr. Opin. Struct. Biol.* 22, 613 (2012).
71. A. Marinelli, M. Dunning, S. Weathersby, E. Hemsing, D. Xiang, G. Andonian, F. O'Shea, J. Miao, C. Hast, and J.B. Rosenzweig, *Phys. Rev. Lett.* 110, 094802 (2013).
72. T. Oroguchi and M. Nakasako, *Phys. Rev. E* 87, 022712 (2013).
73. J.C.H. Spence, U. Weierstall, and M. Howells, *Philos. Trans. R. Soc. Lond A* 360, 875 (2002).
74. J. Miao, T. Ohsuna, O. Terasaki, K.O. Hodgson, and M.A. O'Keefe, *Phys. Rev. Lett.* 89, 155502 (2002).
75. J.M. Zuo, I. Vartanyants, M. Gao, R. Zhang, and L.A. Nagahara, *Science* 300, 1419 (2003).
76. O. Kamimura, K. Kawahara, T. Doi, T. Dobashi, T. Abe, and K. Gohara, *Appl. Phys. Lett.* 92, 024106 (2008).
77. S. Morishita, J. Yamasaki, K. Nakamura, T. Kato, and N. Tanaka, *Appl. Phys. Lett.* 93, 183103 (2008).
78. R. Dronyak, K.S. Liang, Y.P. Stetsko, T.-K. Lee, C.-K. Feng, J.-S. Tsai, and F.-R. Chen, *Appl. Phys. Lett.* 95, 111908 (2009).
79. C.T. Putkunz, A.J. D'Alfonso, A.J. Morgan, M. Weyland, C. Dwyer, L. Bourgeois, J. Etheridge, A. Roberts, R.E. Scholten, K.A. Nugent, and L.J. Allen, *Phys. Rev. Lett.* 108, 073901 (2012).
80. I. Peterson, B. Abbey, C.T. Putkunz, D.J. Vine, G.A. van Riessen, G.A. Cadenazzi, E. Balaur, R. Ryan, H.M. Quiney, I. McNulty, A.G. Peele, and K.A. Nugent, *Opt. Express* 20, 24678 (2012).
81. B. Abbey, L.W. Whitehead, H.M. Quiney, D.J. Vine, G.A. Cadenazzi, C.A. Henderson, K.A. Nugent, E. Balaur, C.T. Putkunz, A.G. Peele, G.J. Williams, and I. McNulty, *Nat. Photonics* 5, 420 (2011).
82. S. Roy, D. Parks, K.A. Seu, R. Su, J.J. Turner, W. Chao, E.H. Anderson, S. Cabrini, and S.D. Kevan, *Nat. Photonics* 5, 243 (2011).
83. A. Szameit, Y. Shechtman, E. Osherovich, E. Bullkich, P. Sidorenko, H. Dana, S. Steiner, E.B. Kley, S. Gazit, T. Cohen-Hyams, S. Shoham, M. Zibulevsky, I. Yavneh, Y.C. Eldar, O. Cohen, and M. Segev, *Nat. Mater.* 11, 455 (2012).
84. J. Bertolotti, E.G. van Putten, C. Blum, A. Lagendijk, W.L. Vos, and A.P. Mosk, *Nature* 491, 232 (2012).

85. K.A. Nugent, D. Paganin, and T.E. Gureyev, *Phys. Today* 54, 27 (2001).
86. A.L. Patterson, *Phys. Rev. B* 46, 372 (1934).
87. D. Sayre, *Acta Crystallogr.* 5, 843 (1952).
88. C.E. Shannon, *Proc. Inst. Radio Eng.* 37, 10 (1949).
89. Y.M. Bruck and L.G. Sodin, *Opt. Commun.* 30, 304 (1979).
90. M.H. Hayes, *IEEE Trans. Accoust. Speech Signal Process* 30, 140 (1982).
91. R. Bates, *Optik* 61, 247 (1982).
92. J. Miao, D. Sayre, and H.N. Chapman, *J. Opt. Soc. Am. A* 15, 1662 (1998).
93. J. Miao, T. Ishikawa, E.H. Anderson, and K.O. Hodgson, *Phys. Rev. B* 67, 174104 (2003).
94. J.R. Fienup, *Opt. Lett.* 3, 27 (1978).
95. J.R. Fienup, *Appl. Opt.* 21, 2758 (1982).
96. V. Elser, *J. Opt. Soc. Am. A* 20, 40 (2003).
97. R. Blankenbecler, *Phys. Rev. B* 69, 064108 (2004).
98. S. Marchesini, *Rev. Sci. Instrum.* 78, 011301 (2007).
99. C.C. Chen, J. Miao, C.W. Wang, and T.K. Lee, *Phys. Rev. B* 59, 064113 (2007).
100. R.W. Gerchberg and W.O. Saxton, *Optik* 35, 237 (1972).
101. C.I. Chou and T.K. Lee, *Acta Crystallogr. Sect. A: Found. Crystallogr.* 58, 42 (2002).
102. C. Song, D. Ramunno-Johnson, Y. Nishino, Y. Kohmura, T. Ishikawa, C.C. Chen, T.K. Lee, and J. Miao, *Phys. Rev. B* 75, 012102 (2007).
103. L. Baghaei, A. Rad, B. Dai, P. Pianetta, R.F.W. Pease, and J. Miao, *J. Vac. Sci. Technol. B* 27, 3192 (2009).
104. R. Xu, S. Salha, K.S. Raines, H. Jiang, C.-C. Chen, Y. Takahashi, Y. Kohmura, Y. Nishino, C. Song, T. Ishikawa, and J. Miao, *J. Synchrotron Radiat.* 18, 293 (2011).
105. A.V. Martin, F. Wang, N.D. Loh, T. Ekeberg, F.R.N.C. Maia, M. Hantke, G. van der Schot, C.Y. Hampton, R.G. Sierra, A. Aquila, S. Bajt, M. Barthelmess, C. Bostedt, J.D. Bozek, N. Coppola, S.W. Epp, B. Erk, H. Fleckenstein, L. Foucar, M. Frank, H. Graafsma, L. Gumprecht, A. Hartmann, R. Hartmann, G. Hauser, H. Hirsemann, P. Holl, S. Kassemeyer, N. Kimmel, M. Liang, L. Lomb, S. Marchesini, K. Nass, E. Pedersoli, C. Reich, D. Rolles, B. Rudek, A. Rudenko, J. Schulz, R.L. Shoeman, H. Soltau, D. Starodub, J. Steinbrener, F. Stellato, L. Strüder, J. Ullrich, G. Weidenspointner, T.A. White, C.B. Wunderer, A. Barty, I. Schlichting, M.J. Bogan, and H.N. Chapman, *Opt. Express* 20, 16650 (2012).
106. J.A. Rodriguez, R. Xu, C.-C. Chen, Y. Zou, and J. Miao, *J. Appl. Crystallogr.* 46, 312 (2013).
107. B. Abbey, G.J. Williams, M.A. Pfeifer, J.N. Clark, C.T. Putkunz, A. Torrance, I. McNulty, T.M. Levin, A.G. Peele, and K.A. Nugent, *Appl. Phys. Lett.* 93, 214101 (2008).
108. S. Boutet and I.K. Robinson, *J. Synchrotron Rad.* 15, 576 (2008).
109. C. Song, R. Bergstrom, D. Ramunno-Johnson, H. Jiang, D. Paterson, M.D. de Jonge, I. McNulty, J. Lee, K. Wang, and J. Miao, *Phys. Rev. Lett.* 100, 025504 (2008).
110. J. Miao, F. Forster, and O. Levi, *Phys. Rev. B* 72, 052103 (2005).
111. D. Attwood, *Soft X-rays and Extreme Ultraviolet Radiation: Principles and Applications* (Cambridge: Cambridge University Press, 1999).
112. T. Popmintchev, M.-C. Chen, P. Arpin, M.M. Murnane, and H.C. Kapteyn, *Nat. Photoics* 4, 822 (2010).
113. R.A. Bartels, A. Paul, H. Green, H.C. Kapteyn, M.M. Murnane, S. Backus, I.P. Christov, Y. Liu, D. Attwood, and C. Jacobsen, *Science* 297, 376 (2002).
114. J.J. Rocca, *Rev. Sci. Instrum.* 70, 3799 (1999).
115. F. Brizuela, I.D. Howlett, S. Carbajo, D. Peterson, A. Sakdinawat, L. Yanwei, D.T. Attwood, M.C. Marconi, J.J. Rocca, and C.S. Menoni, *IEEE J. Sel. Top. Quant. Electron.* 18, 434 (2012).
116. S. Backus, C.G. Durfee III, M.M. Murnane, and H.C. Kapteyn, *Rev. Sci. Instrum.* 69, 1207 (1998).
117. I. McKinnie and H. Kapteyn, *Nat. Photonics* 4, 149 (2010).
118. T. Brabec and F. Krausz, *Rev. Mod. Phys.* 72, 545 (2000).
119. C.A. Brewer, F. Brizuela, P. Wachulak, D.H. Martz, W. Chao, E.H. Anderson, D.T. Attwood, A.V. Vinogradov, I.A. Artyukov, and A.G. Ponomareko, *Opt. Lett.* 33, 518 (2008).
120. P.W. Wachulak, M.C. Marconi, R.A. Bartels, C.S. Menoni, and J.J. Rocca, *J. Opt. Soc. Am. B* 25, 1811 (2008).
121. G. Vaschenko, C. Brewer, F. Brizuela, Y. Wang, M.A. Larotonda, B.M. Luther, M.C. Marconi, J.J. Rocca, C.S. Menoni, and E.H. Anderson, *Opt. Lett.* 31, 1214 (2006).
122. Y. Wang, E. Granados, F. Pedaci, D. Alessi, B. Luther, M. Berrill, and J.J. Rocca, *Nat. Photonics* 2, 94 (2008).
123. J.J. Rocca, C.H. Moreno, M.C. Marconi, and K. Kanizay, *Opt. Lett.* 24, 420 (1999).
124. J. Seres, E. Seres, A.J. Verhoef, G. Tempea, C. Streli, P. Wobrauschek, V. Yakovlev, A. Scrinzi, C. Spielmann, and F. Krausz, *Nature* 433, 596 (2005).
125. A.L. Cavalieri, N. Muller, T. Uphues, V.S. Yakovlev, A. Baltuska, B. Horvath, B. Schmidt, L. Blumel, R. Holzwarth, S. Hendel, M. Drescher, U. Kleineberg, P.M. Echenique, R. Kienberger, F. Krausz, and U. Heinzmann, *Nature* 499, 1029 (2007).
126. Z. Chang and P. Corkum, *J. Opt. Soc. Am. B* 27, B9 (2010).
127. T. Popmintchev, M.-C. Chen, D. Popmintchev, P. Arpin, S. Brown, S. Ališauskas, G. Andriukaitis, T. Balčiunas, O.D. Mücke, A. Pugzlys, A. Baltuška, B. Shim, S.E. Schrauth, A. Gaeta, C. Hernández-García, L. Plaja, A. Becker, A. Jaron-Becker, M.M. Murnane, H.C. Kapteyn, S. Alisauskas, T. Balciunas, and A. Baltuska, *Science* 336, 1287 (2012).
128. T. Ditmire, E.T. Gumbrell, R.A. Smith, J.W.G. Tisch, D.D. Meyerhofer, and M.H.R. Hutchinson, *Phys. Rev. Lett.* 77, 4756 (1996).
129. A. L'Huillier and P. Balcou, *Phys. Rev. Lett.* 70, 774 (1993).
130. P.B. Corkum, *Phys. Rev. Lett.* 71, 1994 (1993).
131. M. Lewenstein, P. Balcou, M.Y. Ivanov, A. L'Huillier, and P.B. Corkum, *Phys. Rev. A* 49, 2117 (1994).
132. T. Popmintchev, M.-C. Chen, O. Cohen, M.E. Grisham, J.J. Rocca, M.M. Murnane, and H.C. Kapteyn, *Opt. Lett.* 33, 2128 (2008).
133. P. Balcou and A. L'Huillier, *Phys. Rev. A* 47, 1447 (1993).
134. A. Rundquist, C.G. Durfee III, Z. Chang, C. Herne, S. Backus, M.M. Murnane, and H.C. Kapteyn, *Science* 280, 1412 (1998).
135. A. Paul, E.A. Gibson, Z. Xiaoshi, A. Lytle, T. Popmintchev, Z. Xibin, M.M. Murnane, I.P. Christov, and H.C. Kapteyn, *IEEE J. Sel. Top. Quant. Electron.* 42, 14 (2006).
136. A.L. Lytle, X. Zhang, R.L. Sandberg, O. Cohen, H.C. Kapteyn, and M.M. Murnane, *Opt. Express* 16, 6544 (2008).
137. A. Paul, R.A. Bartels, R. Tobey, H. Green, S. Weiman, I.P. Christov, M.M. Murnane, H.C. Kapteyn, and S. Backus, *Nature* 421, 51 (2003).
138. M. Wieland, R. Frueke, T. Wilhein, C. Spielmann, M. Pohl, and U. Kleineberg, *Appl. Phys. Lett.* 81, 2520 (2002).
139. P.W. Wachulak, R.A. Bartels, M.C. Marconi, C.S. Menoni, J.J. Rocca, Y. Lu, and B. Parkinson, *Opt. Express* 14, 9636 (2006).
140. P.W. Wachulak, M.C. Marconi, R.A. Bartels, C.S. Menoni, and J.J. Rocca, *Opt. Express* 15, 10622 (2007).
141. F. Brizuela, G. Vaschenko, C. Brewer, M. Grisham, C. Menoni, M. Marconi, J. Rocca, W. Chao, J. Liddle, and E. Anderson, *Opt. Express* 13, 3983 (2005).
142. J. Spence, *Nature* 449, 553 (2007).
143. D.F. Gardner, B. Zhang, M.D. Seaberg, L.S. Martin, D.E. Adams, F. Salmassi, E. Gullikson, H. Kapteyn, and M. Murnane, *Opt. Express* 20, 19050 (2012).
144. B.L. Henke, E.M. Gullikson, and J.C. Davis, *At. Data Nucl. Data Tables* 54, 181 (1993).
145. C. La-O-Vorakiat, M. Siemens, M.M. Murnane, H.C. Kapteyn, S. Mathias, M. Aeschlimann, P. Grychtol, R. Adam, C.M. Schneider, J.M. Shaw, H. Nembach, and T.J. Silva, *Phys. Rev. Lett.* 103, 257402 (2009).

146. C. La-O-Vorakiat, E. Turgut, C.A. Teale, H.C. Kapteyn, M.M. Murnane, S. Mathias, M. Aeschlimann, C.M. Schneider, J.M. Shaw, H.T. Nembach, and T.J. Silva, *Phys. Rev. X* 2, 11005 (2012).
147. B. Vodungbo, J. Gautier, G. Lambert, A.B. Sardinha, M. Lozano, S. Sebban, M. Ducousso, W. Boutu, K. Li, B. Tudu, M. Tortarolo, R. Hawaldar, R. Delaunay, V. López-Flores, J. Arabski, C. Boeglin, H. Merdji, P. Zeitoun, and J. Lüning, *Nat. Commun.* 3, 999 (2012).
148. S. Mathias, C. La-O-Vorakiat, P. Grychtol, P. Granitzka, E. Turgut, J.M. Shaw, R. Adam, H.T. Nembach, M.E. Siemens, S. Eich, C.M. Schneider, T.J. Silva, M. Aeschlimann, M.M. Murnane, and H.C. Kapteyn, *PNAS* 109, 4792 (2012).
149. D. Rudolf, C. La-O-Vorakiat, M. Battiato, R. Adam, J.M. Shaw, E. Turgut, P. Maldonado, S. Mathias, P. Grychtol, H.T. Nembach, T.J. Silva, M. Aeschlimann, H.C. Kapteyn, M.M. Murnane, C.M. Schneider, and P.M. Oppeneer, *Nat. Commun.* 3, 1037 (2012).
150. J. Schwenke, A. Mai, M. Miranda, X. He, G. Genoud, A. Mikkelsen, S.-G. Pettersson, A. Persson, and A. L'Huillier, *J. Mod. Opt.* 55, 2723 (2008).
151. D. Gauthier, M. Guizar-Sicairos, X. Ge, W. Boutu, B. Carre, J.R. Fienup, and H. Merdji, *Phys. Rev. Lett.* 105, 93901 (2010).
152. H.C. Kang, H.T. Kim, S.S. Kim, C. Kim, T.J. Yu, S.K. Lee, C.M. Kim, I.J. Kim, J.H. Sung, K.A. Janulewicz, J. Lee, and D.Y. Noh, *Opt. Lett.* 37, 1688 (2012).
153. E.B. Malm, N.C. Monserud, C.G. Brown, P.W. Wachulak, H. Xu, G. Balakrishnan, W. Chao, E. Anderson, and M.C. Marconi, *Opt. Express* 21, 9959 (2013).
154. N. Lei, *J. Phys. Condens. Matter* 19(21), 216215 (2007). doi:10.1088/0953-8984/19/21/216215.
155. N. Nakajima, *J. Opt. Soc. Am. A* 26, 2172 (2009).
156. C.-C. Chen, H. Jiang, L. Rong, S. Salha, R. Xu, T.G. Mason, and J. Miao, *Phys. Rev. B* 84, 224104 (2011).
157. P. Colosimo, G. Doumy, C.I. Blaga, J. Wheeler, C. Hauri, F. Catoire, J. Tate, R. Chirla, A.M. March, G.G. Paulus, H.G. Muller, P. Agostini, and L.F. DiMauro, *Nat. Phys.* 4, 386 (2008).
158. H. Xiong, H. Xu, Y. Fu, J. Yao, B. Zeng, W. Chu, Y. Cheng, Z. Xu, E.J. Takahashi, K. Midorikawa, X. Liu, and J. Chen, *Opt. Lett.* 34, 1747 (2009).
159. T. Popmintchev, M.-C. Chen, A. Bahabad, M. Gerrity, P. Sidorenko, O. Cohen, I.P. Christov, M.M. Murnane, and H.C. Kapteyn, *PNAS* 106, 10516 (2009).
160. M.C. Chen, P. Arpin, T. Popmintchev, M. Gerrity, B. Zhang, M. Seaberg, D. Popmintchev, M.M. Murnane, and H.C. Kapteyn, *Phys. Rev. Lett.* 105, 173901 (2010).
161. Y. Takahashi, Y. Nishino, R. Tsutsumi, H. Kubo, H. Furukawa, H. Mimura, S. Matsuyama, N. Zettsu, E. Matsubara, T. Ishikawa, and K. Yamauchi, *Phys. Rev. B* 80, 54103 (2009).
162. J.M. Rodenburg, *Proc. SPIE* 8678, 867809 (2012).
163. A.J. Morgan, A.J. D'Alfonso, P. Wang, H. Sawada, A.I. Kirkland, and L.J. Allen, *Phys. Rev. B* 87, 094115 (2013).
164. L. De Caro, E. Carlino, G. Caputo, P.D. Cozzoli, and C. Giannini, *Nat. Nanotechnol.* 5, 360 (2010).
165. J. Gulden, O.M. Yefanov, E. Weckert, and I.A. Vartanyants, *AIP Conf. Proc.* 1365, 42 (2011).
166. M.C. Scott, C.-C. Chen, M. Mecklenburg, C. Zhu, R. Xu, P. Ercius, U. Dahmen, B.C. Regan, and J. Miao, *Nature* 483, 444 (2012).
167. C.-C. Chen, C. Zhu, E.R. White, C.-Y. Chiu, M.C. Scott, B.C. Regan, L.D. Marks, Y. Huang, and J. Miao, *Nature* 496, 74 (2013).